Catalysis Today 151 (2010) 386–394

Contents lists available at ScienceDirect

Catalysis Today

journal homepage: www.elsevier.com/locate/cattod

Dual-catalyst aftertreatment of lean-burn engine exhaust

Burcu Mirkelamoglu, Meimei Liu, Umit S. Ozkan *

140 W. 19th Avenue, Department of Chemical and Biomolecular Engineering, The Ohio State University, Columbus, OH 43210, USA

ARTICLE INFO

Article history:
Available online 18 February 2010

Keywords:
XPS
XRD
Dispersion
Lean NO_x reduction
Sulfated zirconia
Palladium
Cobalt
NO oxidation

ABSTRACT

Pd/SZ catalysts prepared by a sol–gel technique were investigated with regards to their NO_2 selective catalytic reduction activity for application in a novel integrated NO-CO-hydrocarbon oxidation and NO_x-selective catalytic reduction system for aftertreatment of lean-burn natural gas reciprocating engine exhaust. The dual-catalyst system consists of a mechanical mixture of a non-noble-metal based oxidation catalyst component (Co/ZrO_2) for elimination of carbon monoxide and unburned hydrocarbons and oxidation of NO to NO_2 and a reduction catalyst component (Pd/SZ) for selective catalytic reduction (SCR) of NO_2 with CH_4. The effect of sol–gel preparation parameters on the activity of Pd/SZ was investigated. The zirconium alkoxide concentration was varied between 0.3 M and 1.3 M during preparation of the Pd/SZ series of catalysts while other sol–gel parameters, such as hydrolysis and zirconium-to-sulfur precursor ratios and palladium loadings were kept constant. Pd/SZ prepared with the lowest concentration of alkoxide was mainly composed of metastable tetragonal zirconia while increasing alkoxide concentration resulted in decreased stability of t-ZrO_2 as evidenced by formation of m-ZrO_2 domains. Crystal phase of ZrO_2 was observed to have a significant effect on Pd dispersion. Palladium dispersion increased with increasing concentration of the monoclinic phase. The best performing Pd/SZ catalyst was further tested as the NO_x reduction catalyst component for simulated lean exhaust treatment over the dual-catalyst scheme where, N_2 yields in excess of 90% along with significant conversions of CO, CH_4, C_2H_6 and C_3H_8 were achieved at 450 °C. The NO_x reduction activity of Pd/SZ was significantly inhibited in the presence of water vapor. The presence of oxidation catalyst in close proximity to the reduction catalyst was shown to act to offset the effect of water vapor. Above 70% N_2 yield was achieved at 450 °C in the presence of 7% water vapor during simulated lean exhaust treatment over the dual-catalyst system.

1. Introduction

Natural gas-fired reciprocating engines operating in the lean combustion regime are widely employed for distributed power generation since this technology is simple, inexpensive and produces significantly cleaner exhaust emissions than engines operating in the rich combustion regime [1]. Although the lean-burn natural gas engine exhaust is cleaner, it still contains significant levels of carbon monoxide, unburned hydrocarbons and nitrogen oxides (NO_x) that necessitate aftertreatment of the engine-out exhaust stream. Hydrocarbon-SCR presents a promising alternative for NH_3-SCR, which is the currently employed technology for emissions abatement from stationary sources since hydrocarbons are readily available in the exhaust stream and their use would eliminate several issues centered around the use of ammonia, such as ammonia slip and direct oxidation, corrosion of the downstream equipment due to ammonium salts and lack of ammonia infrastructure [2]. Methane is the major component of natural gas and is also readily available in the exhaust stream of the natural gas reciprocating engine. However, effective use of methane as the reducing agent in an aftertreatment system is a challenge since, under the operating conditions of the aftertreatment system, NO_x reduction with methane receives significant competition from combustion of the hydrocarbon in the presence of excess oxygen [3,4].

Nishizaka and Misono [5,6] were the first to report that palladium-based zeolitic catalysts showed high selectivity for catalytic reduction of NO_x with CH_4 under lean conditions. Palladium based catalysts supported on zeolitic supports such as mordenite [7,8] and ZSM-5 [9–11] have been shown to exhibit high CH_4-SCR activity. Despite their high activity and selectivity in catalytic reduction of NO_x with hydrocarbons, zeolite-based catalysts suffered from formation of bulky PdO particles, which are active for methane combustion [12,13], and loss of dispersion with time-on-stream under hydrothermal conditions [13–15]. Noble-metal catalysts supported on acidic oxide supports are widely investigated for selective catalytic reduction of NO_x with CH_4 under lean conditions as metal oxide supports are not prone to structural damage, like the zeolite-based catalysts are, in the presence of steam [16]. Acidic supports are able to stabilize

* Corresponding author. Tel.: +1 614 292 6623; fax: +1 614 292 3769.
E-mail address: ozkan.1@osu.edu (U.S. Ozkan).

0920-5861/$ – see front matter © 2010 Elsevier B.V. All rights reserved.
doi:10.1016/j.cattod.2009.12.014

palladium in the form of Pd^{2+} ions which were shown to be active sites for NO_x reduction [17]. Sulfated zirconia has attracted significant attention since protons associated with surface sulfate groups can serve as anchoring sites for Pd^{2+} [18].

Sulfated zirconia is most commonly prepared in two steps through sulfuric acid impregnation of $Zr(OH)_4$, which was obtained through precipitation by ammonia from a solution of $ZrCl_4$ [19,20] or $ZrOCl_2$ [21,22]. A one-step sol–gel route where sulfuric acid was added to zirconium alkoxide solution prior to hydrolysis was also suggested [23]. Tichit et al. [24] compared the activity of SZ prepared through different methods in n-hexane isomerization and reported that sol–gel prepared catalysts had higher sulfate retention and had higher activity. A number of sol–gel preparation parameters such as the protocol followed for sulfate addition [24,25] and hydrolysis ratio [26,27] has been shown to have significant influence on the morphology and activity of SZ catalysts. In addition to sol–gel parameters, application of nucleophilic reagents such as acetic acid and acetylacetone during sol–gel preparation has been reported as an effective method for controlling the morphology of SZ catalysts [26,28]. More recently, Hamouda and Ghorbel [29] reported sol–gel preparation of SZ by *in situ* generation of hydrolysis water through sulfuric acid catalyzed alcohol dehydration. These catalysts showed higher sulfate retention and activity in isomerization reactions. Sol–gel method also enables one-pot synthesis of SZ supported noble-metal catalysts [30,31].

We have previously reported a novel integrated oxidation/selective catalytic reduction approach that utilizes an oxidation catalyst component and a NO_x reduction catalyst component to combine three distinct catalytic functions, namely, NO_x reduction, CO oxidation and hydrocarbon combustion in a single aftretreatment unit [32,33]. The integrated dual-catalyst concept for lean exhaust aftertreatment is a versatile approach that can be fine-tuned to fit in for aftertreatment of any engine exhaust by modification of the catalyst components to effectively utilize whatever hydrocarbon(s) is available in the exhaust stream as the reducing agent. The dual-catalyst approach aims at overcoming the competition that NO-SCR receives from hydrocarbon combustion during lean NO_x aftertreatment by converting NO to NO_2 and taking advantage of the stronger oxidizing potential of NO_2 relative to NO for competing with oxygen for the use of hydrocarbon reducing agent. NO oxidation to NO_2 is an exothermic and reversible reaction and therefore, is thermodynamically limited at high temperatures [34]. The dual-catalyst system is capable of pushing the equilibrium forward towards products as NO; that is produced in close proximity to the reduction catalyst, is removed from the system through SCR reaction. In the dual-catalyst scheme, the oxidation catalyst assumes a multi-functional role by taking part in the elimination of carbon monoxide and hydrocarbons that have not been consumed in NO_x reduction over the reduction catalyst component [32].

Catalyst development studies for the dual-catalyst integrated system were undertaken simultaneously. Co-based NO oxidation catalyst formulations have been developed and 10% Co/ZrO_2 has been demonstrated to achieve equilibrium conversions at temperatures as low as 250 °C [35]. Initial work on reduction catalyst component involved a two-step incipient wetness impregnation procedure where commercial monoclinic ZrO_2 was impregnated with ammonium sulfate and palladium chloride in two separate steps. The prepared catalysts have been shown to give good NO_2 reduction activity with CH_4 around 375–400 °C [36]. A dual-catalyst bed consisting of a mixture of 10% Co/ZrO_2 and 0.3% Pd/SZ was tested under simulated lean exhaust conditions and achieved significantly higher N_2 yields than NO-SCR over the reduction catalyst alone [32]. Sol–gel method for single-step preparation of Pd/SZ was utilized in a later contribution and the effect of palladium loading and calcination temperature of the dried gel on the NO_2-SCR activity was investigated. Catalysts prepared by this route have been shown to give significant NO_2-SCR activity in 400–450 °C region [30].

In this contribution, we report studies on the effect of alkoxide concentration on the morphological and catalytic properties on Pd/SZ. Pd/SZ samples were prepared with different alkoxide concentrations while hydrolysis and zirconium-to-sulfur precursor ratios were maintained constant. X-ray diffraction, X-ray photoelectron spectroscopy, N_2-physisorption and H_2 pulsed chemisorption experiments were performed on the samples along with steady-state NO_x reduction activity tests to correlate SCR activity with morphological properties. The best performing Pd/SZ sample was further tested for activity in simulated lean exhaust treatment over the dual-catalyst scheme consisting of a mixture of oxidation and reduction catalyst components.

2. Experimental

2.1. Catalyst preparation and characterization

Palladium supported on sulfated zirconia prepared through a one-pot sol–gel route described earlier [30] was investigated as the NO_x reduction catalyst component of the dual-catalyst scheme. The procedure uses palladium acetate (Aldrich), zirconium propoxide (70% solution in n-propanol, Aldrich) and sulfuric acid (Fisher Sci.) as the precursors, acetic acid (Fisher Sci.) as the controlled hydrolysis agent and n-propanol (Fisher Sci.) as the solvent. Palladium loading was kept constant at 0.3% for all of the samples. A calculated amount of palladium acetate was dissolved in n-propanol and calculated amounts of zirconium propoxide and sulfuric acid were added under constant stirring. The final concentrations of zirconium propoxide ($Zr(Pr)_4$) and sulfuric acid in the sol were varied while keeping $[Zr(Pr)_4]$-to-$[H_2SO_4]$ ratio constant at 2 to investigate the effect of alkoxide concentration on sulfate anchoring on to the zirconium oxide network and on catalytic activity. The final alkoxide molar concentrations are given in Table 1, where numbers in parenthesis next to Pd/SZ represent the molar concentration of alkoxide in the sol during the preparation of that catalyst.

The solution containing zirconium propoxide and sulfuric acid along with palladium acetate and n-propanol was stirred for 30 min and acetic acid in the amount to give a hydrolysis ratio of 4 was added using a syringe pump set to deliver 0.2 ml of acetic acid per minute. A viscous gel formed following the addition of acetic acid. The gel was dried overnight oven at 110 °C in a drying oven. The dried gel was ground and calcined at 700 °C for 4 h under continuous flow of oxygen and then, ground to a fine powder.

The NO oxidation catalyst component of the dual-catalyst system (10% Co/ZrO_2) was prepared through a conventional incipient wetness impregnation route using commercial monoclinic zirconia (m-ZrO_2) supplied by Saint-Gobain in pelletized form. The support material was ground and sieved to save the 100/150 mesh cut (0.149–0.105 mm). The support was then calcined in air for 3 h at 500 °C. For the impregnation of the calcined support, a calculated amount of cobalt precursor (cobalt nitrate hexahydrate—Aldrich) to yield 10% Co loading in the final catalyst, was

Table 1
Sol–gel parameters, surface areas and pore volumes of Pd/SZ.

Catalyst	$[Zr(Pr)_4]$	$\frac{[Zr(Pr)_4]}{[H_2SO_4]}$	$\frac{[CH_3COOH]}{[Zr(Pr)_4]}$	Surface area (m^2/g)	Pore volume (m^3/g)
Pd/SZ (0.3)	0.3	2	4	71	0.21
Pd/SZ (0.6)	0.6	2	4	73	0.21
Pd/SZ (1.0)	1.0	2	4	67	0.23
Pd/SZ (1.3)	1.3	2	4	60	0.18

dissolved in deionized water. Impregnation of the support with this solution was carried out in two steps to improve catalyst homogeneity. After each impregnation, the catalyst was dried at 110 °C overnight. After the second drying, the catalysts were calcined in air at 500 °C for 3 h. Extensive characterization on the oxidation catalyst component through BET surface area measurements, temperature programmed techniques, X-ray photoelectron spectroscopy (XPS), X-ray diffraction (XRD), laser Raman spectroscopy (LRS) and diffuse reflectance Fourier transform infrared spectroscopy (DRIFTS) has been reported previously [35].

Static surface area and pore volume measurements were made using a Micromeritics ASAP 2010 accelerated surface area and porosimetry instrument, using N_2 physisorption technique. Prior to analysis, samples were degassed overnight at 130 °C under a vacuum of 3 μmHg. The specific surface areas were determined by the Brunauer–Emmett–Teller (BET) method using the adsorption branch of the N_2 adsorption/desorption isotherm. The specific pore volumes of the samples were determined the Barrett–Joiner–Halenda (BJH) method using the desorption branch of the isotherm.

XRD patterns of the Pd/SZ samples were collected on a Bruker D8 Advance X-ray diffractometer. The diffraction patterns were collected in the 20–70° diffraction angle range using Cu Kα radiation (λ = 1.5418 Å) through a tube operated at 40 kV and 50 mA. International Center for Diffraction Data (ICDD) database was used for crystalline phase identification through the collected diffraction patterns. Toraya et al.'s method [37] was utilized to calculate the volume fraction of tetragonal ZrO_2 phase when m- and t-phases of ZrO_2 coexisted. This method makes use of the intensities of [$\bar{1}$ 1 1] and [1 1 1] diffraction lines of m-ZrO_2 and [1 1 1] diffraction line of t-ZrO_2 to calculate volume fraction of the phases when m- and t-phases coexist. The crystallite sizes of the samples were calculated through the broadening of the diffraction peaks using Scherrer's equation. [$\bar{1}$ 1 1] and [1 0 1] diffraction lines were used for calculation of the crystallite sizes of m- and t-ZrO_2 phases, respectively.

Transmission electron microscopy (TEM) images were collected in brightfield mode on a Phillips Tecnai F20 instrument with FEG operated at a voltage of 200 kV. The sample was dispersed in ethanol and deposited onto 200 mesh copper grid coated with lacey carbon following sonication for 20 min.

The X-ray photoelectron spectra of the Pd/SZ samples were collected in a Kratos AXIS Ultra X-ray photoelectron spectrometer, using monochromatized Al Kα (1486.7 eV) radiation from a X-ray source operated at 13 kV and 10 mA. Samples were ground on to a double sided carbon tape directly after calcination and transferred to the UHV chamber of the XPS instrument. Survey X-ray photoelectron spectra were collected before region scans, where carbon was observed to be the only contaminant on the surface. When necessary, the charge neutralizer was operated at a current of 2.0A and a filament bias of 1.3 V. The collected data were corrected for charge shifting using standard C 1s binding energy of 284.5 eV. Concurrent sweeps of high resolution X-ray photoelectron spectra were collected for Zr 3d, S 2p, O 1s and C 1s regions at an electron pass energy of 20 eV. Data analysis with background subtraction and curve fitting was done on XPS Peak 4.1. For quantitative comparison of the surface concentration of different species, the counts per second were divided by the number of sweeps and the transmission value at the respective binding energy. XPS peak areas of each species were corrected with the respective instrumental atomic sensitivity factors.

Palladium dispersion on Pd/SZ samples was measured by hydrogen chemisorption on an automated catalyst characterization system (Autochem 2910, Micromeritics) following the procedure outlined by Maffucci et al. [38]. For each run, 150 mg of catalyst sample was packed inside a 1/4 in. quartz U-tube reactor using quartz wool plugs and reduced with H_2 (45 sccm) at 300 °C for 2 h. The reactor was then flushed with N_2 (45 sccm) at the same temperature for another 30 min and the sample was cooled down to 150 °C under the same atmosphere. At 150 °C the system was pulsed with 0.15 ml pulses of O_2 to remove physisorbed hydrogen from the surface without re-oxidizing the surface. Following oxygen pulses, the system was flushed with N_2 for an hour. Hydrogen chemisorption was carried out by 0.15 ml pulses of H_2 at 150 °C to prevent formation of palladium hydride. Nitrogen was used as the carrier gas during all of the pulses. The evolution of H_2 from the reactor was monitored by a thermal conductivity detector (TCD). The amount of chemisorbed hydrogen was calculated as: $V_{\text{Hydrogen}} = V_{\text{loop}} \sum_{i=1-n} [1 - (A_i/A_0)]$, where A_i is the area under the ith injection and A_0 is the area under the peak at steady-state. Palladium dispersion was calculated assuming a hydrogen chemisorption stoichiometry (H/Pd_s) of 1.

2.2. Catalytic activity testing

A fixed bed, 1/4 in. OD stainless steel reactor system operating at ambient pressure was used for steady-state catalytic activity measurements. For each run, samples were packed inside the reactor using quartz wool plugs. The temperature of the catalyst bed was measured and controlled by a K-type thermocouple in contact with the quartz wool plug at the upstream side of the catalyst bed and an Omega 76000 temperature controller. Independent Brooks 5850E mass flow controllers connected to Brooks 0154 electronics control boxes were used to control gas flow rates. Reactant gases were supplied from Praxair and used without any further treatment. Separation and quantification of O_2, N_2, N_2O, CH_4, C_2H_6, C_3H_8, CO and CO_2 was performed using an online microGC (Varian, CP4900), equipped with molecular sieve 5A and PoraPLOT columns. A chemiluminescence $NO/NO_2/NO_x$ analyzer (Thermo Environmental, 42iHL) connected in series to the micro GC was used for monitoring NO_x species. Reactant conversions were calculated as $(1 - C_i/C_i^0) \times 100\%$. Yields for N-containing compounds were calculated as $(\varphi \times C_i/C_{NO_x}^0) \times 100\%$ where, C_i and C_i^0 are inlet and outlet concentrations of species i, respectively and φ is the stoichiometric factor, which is 2 for N_2O and N_2 and 1 for NO. All carbon and nitrogen balances were always better than 97%. Reported conversions and yields are representative of the catalyst activity after steady-state is reached, which usually took 1 h.

The NO_x reduction activity of the Pd/SZ samples was tested on an equal surface area basis in the temperature range between 250 and 600 °C. The catalysts were pretreated in 10% O_2/He (45 sccm) at 400 °C for 30 min before the activity tests. Then the reactor was cooled to 250 °C under the same atmosphere and the reaction feed was introduced. Initial catalytic activity tests were performed in 1000 ppm NO (or NO_2), 3000 ppm CH_4, and 10% O_2 in balance He at a GHSV of 20,000 h^{-1}. Further catalytic activity tests were carried out under simulated lean exhaust, which consisted of 400 ppm NO, 1700 ppm CH_4, 200 ppm C_2H_6, 100 ppm C_3H_8, 600 ppm CO, 6% CO_2 and 10% O_2 in helium at a GHSV of 20,000 h^{-1}.

For experiments involving simulated lean exhaust treatment over the dual-catalyst system, samples of the oxidation and reduction catalysts were thoroughly mixed before being placed into the reactor. In order to compare the reduction efficiency, a constant mass of reduction catalyst (200 mg) was used during the NO/NO_2 reduction and dual bed experiments, while the amount of the oxidation catalyst was varied. The samples were mixed with 100/150 mesh cut quartz powder to keep the bed volume constant during reactions where the amount of the oxidation catalyst component was varied.

The activity of the reduction catalyst component as well as the dual-catalyst mixed bed was also studied in the presence of water

vapor. The abovementioned experimental setup was used for these studies and water vapor was supplied to the system by bubbling helium through a heated bubbler containing de-ionized water. The temperature of the bubbler was monitored and controlled precisely by a temperature controller. Gas lines in contact with water vapor containing stream was heated using heating tapes in order to avoid water condensation in the lines. The feed composition for these experiments were 1000 ppm NO (or NO_2), 3000 ppm CH_4, 10% O_2 and 0–7% H_2O in He. The effect of water vapor on simulated lean exhaust treatment over dual-catalyst mixed bed was also investigated. The simulated lean feed constituted 400 ppm NO, 1700 ppm CH_4, 200 ppm, 100 ppm C_3H_8, 600 ppm CO, 6% CO_2, 10% O_2 and 0–7% H_2O in helium.

3. Results and discussion

3.1. Catalyst characterization: effect of alkoxide concentration

N_2 adsorption/desorption isotherms (not shown) collected for the Pd/SZ catalysts are in line with a type IV system according to the IUPAC classification indicating mesoporous materials with pores in 2–50 nm range. Table 1 shows the specific surface areas and pore volumes of the prepared catalysts. The calculated BET surface area values are in agreement with previous results on this series of catalysts [30]. The BET surface areas of the Pd/SZ samples were inversely correlated with the alkoxide concentration in the sol. Similar observations on the effect of alkoxide concentration on the surface area of sol–gel prepared SO_4^{2-}/ZrO_2 has also been reported by Signoretto et al. [28]. As it will be discussed below, changing alkoxide concentration in the sol during catalyst preparation resulted in significant changes in the catalyst structure, especially in the major crystalline phases and particle sizes such as the formation of denser m-ZrO_2, which could be related to the change in the specific surface areas. The BJH adsorption calculations indicate a pore size distribution centered at 10 ± 0.5 nm for all samples.

X-ray diffraction was used to investigate the effect of alkoxide concentration on the formation of crystalline phases in Pd/SZ samples. Fig. 1 shows the XRD patterns of the four Pd/SZ samples. Over Pd/SZ (0.3), formation of tetragonal zirconia (ICDD # 17-923), as evidenced by [1 1 1] ($2\theta = 30.2^\circ$), [0 0 2] ($2\theta = 34.5^\circ$), [2 0 0] ($2\theta = 35.3^\circ$), [2 2 0] ($2\theta = 50.4^\circ$), [1 1 3] ($2\theta = 58.6^\circ$), [3 1 1] ($2\theta = 59.8^\circ$) and [2 2 2] ($2\theta = 62.1^\circ$) diffraction lines was observed in the XRD pattern (Fig. 1a). Although the major crystal phase was tetragonal zirconia, formation of the monoclinic zirconia domains (ICDD # 37-1484), which could be identified by the [$\bar{1}$ 1 1], [1 1 0] and [1 1 1] diffraction lines at 24.1°, 28.5° and 31.5° was also observed over this sample. No diffraction lines associated with Pd containing phases were resolved on any of the diffraction patterns since the Pd loading of the catalysts is below the sensitivity of XRD technique. Diffraction peaks associated with m-ZrO_2 increased in intensity with increasing alkoxide concentration (Fig. 1b–d) suggesting formation of larger monoclinic zirconia domains with increasing alkoxide concentration. In the XRD pattern of Pd/SZ (1.3), where highest contribution from m-ZrO_2 phase was present, diffraction peaks located at 24.5°, 28.2°, 31.5°, 40.8°, 44.8°, 54.3° and 55.4° which could be associated with [0 1 1], [$\bar{1}$ 1 1], [1 1 1], [$\bar{1}$ 1 2], [2 1 1], [0 0 3] and [3 1 0] planes of m-ZrO_2, respectively, were resolved along with the above mentioned diffractions from t-ZrO_2 phase.

The relative amount of tetragonal phase with respect to monoclinic phase was calculated using the method established by Toraya et al. [37]. Table 2 shows the volume fraction of the metastable tetragonal phase in the Pd/SZ samples. Significant amount of metastable tetragonal zirconia phase was observed over the Pd/SZ sample prepared with the lowest alkoxide concentration.

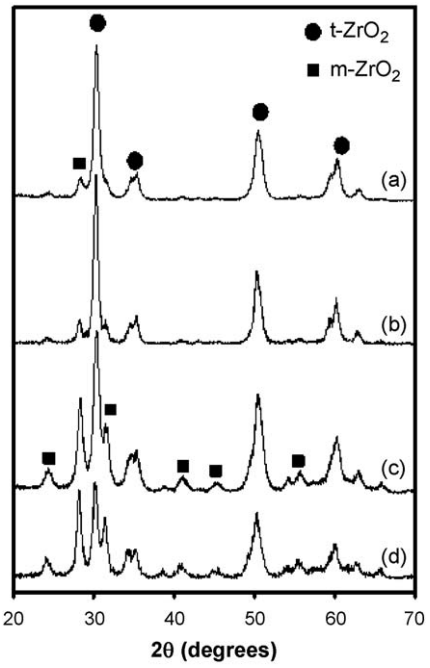

Fig. 1. XRD patterns of (a) Pd/SZ (0.3), (b) Pd/SZ (0.6), (c) Pd/SZ (1.0) and (d) Pd/SZ (1.3)

The decrease in the volume fraction of the metastable tetragonal phase indicates that t- to m-transition takes place at a higher rate with increasing alkoxide concentration and the stabilizing effect of sulfate groups diminishes.

The crystallite sizes of both monoclinic and tetragonal zirconia domains were calculated using Scherrer equation and are presented in Table 2. The crystallite size calculations are in agreement with TEM images which further confirm the formation of zirconia domains in the order of 10 nm (Fig. 2). In all of the samples where t-ZrO_2 and m-ZrO_2 phases were observed to coexist, crystallite size calculations showed that the m-ZrO_2 crystallites were larger than t-ZrO_2 crystallites. This observation is in line with the findings of Bailey et al. [39]. Crystallite size calculations also demonstrated that while increasing alkoxide concentration had no effect on the size of t-ZrO_2 crystallites, it resulted in the formation of larger m-ZrO_2 domains. Formation of m-ZrO_2 crystallites that are larger than t-ZrO_2 crystallites is in agreement with the decrease in the surface of the catalysts with increasing alkoxide concentration.

Zirconia has a number of different crystal structures including cubic, tetragonal and monoclinic. Among these structures monoclinic phase is the thermodynamically stable one at room temperature while tetragonal zirconia is stable above 1150 °C and cannot be quenched [40]. During calcination of zirconium precursors, a metastable tetragonal phase is first formed which is then transformed to monoclinic phase at temperatures above 500 °C [41,42]. Although tetragonal zirconia is not stable at low

Table 2
Crystallite size and phase composition of Pd/SZ catalysts determined by XRD.

Catalyst	Crystallite size (nm)		% t-ZrO_2
	t-ZrO_2	m-ZrO_2	
Pd/SZ (0.3)	11.6	–	0.73
Pd/SZ (0.6)	11.3	11.5	0.71
Pd/SZ (1.0)	11.0	13.0	0.42
Pd/SZ (1.3)	11.9	13.7	0.33

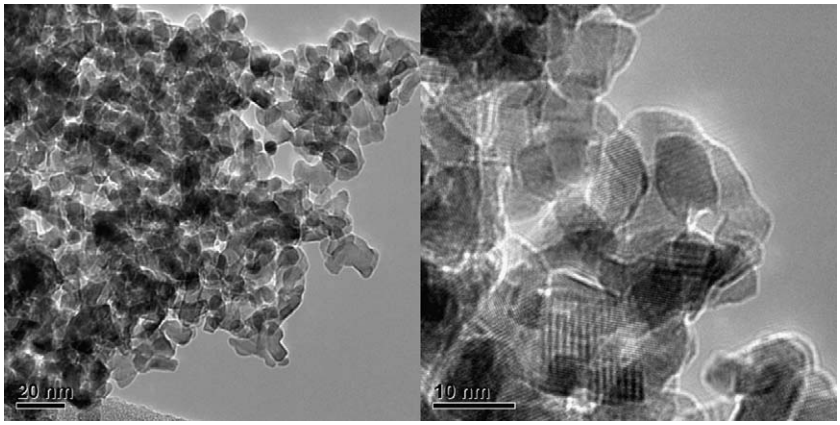

Fig. 2. TEM images of Pd/SZ (1.0).

temperatures various studies in the literature report the existence of a metastable tetragonal phase at room temperature, the presence of which was associated with crystallite size effects [43] or the stabilizing effect of dopants [44]. Presence of metastable tetragonal ZrO_2 phase in the Pd/SZ samples investigated here can be associated with the presence of sulfate, which has also been cited as a stabilizer for t-ZrO_2 phase [26,45,46].

A H_2 pulsed chemisorption technique developed by Maffucci et al. [38] was utilized for obtaining dispersion of palladium over Pd/SZ samples. Table 3 also shows the dispersion of Pd over sulfated zirconia. Despite the decreasing trend in specific surface area of the catalysts (see Table 1) palladium dispersion increased with increasing alkoxide concentration in the sol. Yang et al. [47] observed an increase in Pd dispersion over Pd supported on ZrO_2 containing both m- and t-phases relative to Pd supported on metastable t-ZrO_2 only. It should be noted that palladium dispersion measurements were not intended to assess the oxidation state of palladium during the SCR reaction, but rather to provide an indication of the roles of different crystalline phases of zirconia in stabilizing palladium.

Table 3
Pd dispersion and surface composition of Pd/SZ catalysts.

Catalyst	Pd dispersion (%) (H_2 chemisorption)	S/Zr (XPS)	O/S
Pd/SZ (0.3)	24	0.23	4.19
Pd/SZ (0.6)	41	0.23	4.02
Pd/SZ (1.0)	57	0.20	3.95
Pd/SZ (1.3)	60	0.23	4.09

The chemical states of zirconium, oxygen and sulfur in the Pd/SZ samples were investigated by X-ray photoelectron spectroscopy. The survey spectra of all of the samples were consisted of photopeaks associated with zirconium, sulfur, oxygen and carbon. Fig. 3 shows the core level X-ray photoelectron spectra of Pd/SZ samples in the O 1s, S 2p and Zr 3d regions. In all of the samples, the Zr 3d envelope consisted of a single doublet. Peak fitting of this region showed that this doublet was composed of a single component located at 182.3 eV with a $3d_{5/2}$–$3d_{3/2}$ spin orbit splitting of 2.4 eV. This photopeak is characteristic of Zr^{4+} in zirconium oxide environment [48]. Similarly, the peak fitting of the X-ray photoelectron spectra of S 2p regions of the samples showed the presence of a single component located at 168.8 eV. The splitting between $2p_{3/2}$ and $2p_{1/2}$ was not observed for the S 2p envelope due to close spin orbit splitting for sulfur and low counts in this region arising from the low intrinsic atomic sensitivity factor for this atom. The location of this photopeak is characteristic for sulfur species in sulfate environment [48,49]. In all of the samples, the O 1s envelope was observed as a broad photopeak with a shoulder corresponding to high binding energy region (Fig. 3). Peak fitting in this region showed the presence of contributions from three components which are located at 530, 531.5 and 532.3 eV. In all of the samples, the photopeak located

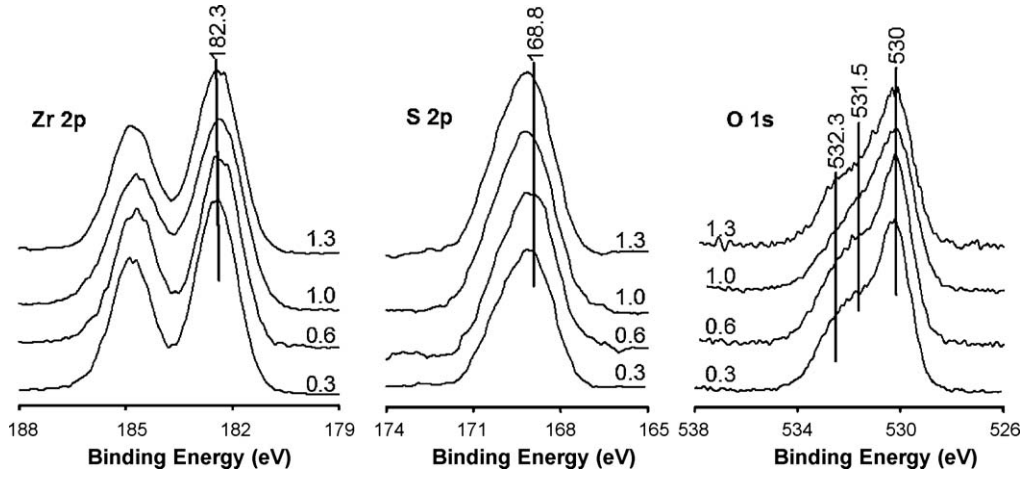

Fig. 3. X-ray photoelectron spectra of Pd/SZ samples.

530 eV had the largest contribution to the O 1s envelope. This photopeak has been associated with oxygen atoms in zirconia matrix. The component at 531.5 eV is characteristic of oxygen coordinated to sulfate atoms. The highest binding energy component located at 532.3 eV has been associated with chemisorbed oxygen and/or hydroxyl groups [50,51].

The surface S/Zr and O/S atomic ratios were calculated for each sample by using the areas under the respective photopeaks and instrumental atomic sensitivity factors. Table 3 shows these ratios. The S/Zr ratios calculated form XPS are almost the same for all of the samples, indicating that changing alkoxide concentration did not have any effect on sulfate retention. During preparation of the catalysts, the $[H_2SO_4]/[Zr(Pr)_4]$ ratio was kept constant at 0.5 while changing the alkoxide concentration in the sol. A sulfate retention of approximately 20% was calculated for all of the samples by making use of the atomic S/Zr ratios obtained through XPS, with the assumption that the sulfate concentration is uniform throughout the catalysts. Similarly, the O/S ratio obtained through taking O 1s component associated with sulfate groups (531.5 eV) into account suggested sulfate stoichiometry for the sulfur species on all of the samples.

3.2. Activity testing

Fig. 4 shows CH_4 conversion and N-containing product distributions as a function of reaction temperature during NO_2 reduction with CH_4 over Pd/SZ samples prepared by changing alkoxide concentration of the sol. Over all of the samples, the N_2 yields increased with temperature going through a maximum in 450–550 °C region. This behavior is typical for NO_x reduction reactions carried out in the presence of excess oxygen and arises from increased rate of consumption of the reducing agent with increasing temperature through combustion which results in its decreased availability for NO_x reduction reaction. The Pd/SZ (0.3) sample achieved a maximum yield of 49% at 550 °C. Over the Pd/SZ (0.6) the temperature of maximum N_2 yield shifted by 50–500 °C and a N_2 yield of 66% was observed over this sample. For the Pd/SZ (1.0) and Pd/SZ (1.3) samples the N_2 yield curves followed each other closely across the whole temperature range reaching N_2 yields in excess of 70% in 450–500 °C region. Corresponding CH_4 conversions are shown in Fig. 4b. The CH_4 conversions over Pd/SZ 0.6, Pd/SZ 1.0 and Pd/SZ 1.3 showed very similar light-off behavior although CH_4 conversions over Pd/SZ 0.6 and Pd/SZ 1.0 were on the average 5–10% lower than over Pd/SZ 1.3. For Pd/SZ 0.3, CH_4 conversions were significantly lower than the other three samples below 550 °C, reaching complete conversion at 600 °C along with the other samples.

Both NO and N_2O are by-products of NO_2 reduction with CH_4 under lean conditions over Pd/SZ based catalysts. Another possible by-product of NO_2-CH_4 reaction is ammonia. To investigate the possibility of ammonia formation as a by-product over Pd/SZ based catalysts, formation and transformation of surface species were studied with *in-situ* DRIFT spectroscopy (not shown) and formation of ammonia over Pd/SZ samples was not observed during these studies. Fig. 4(c) and (d) shows the distribution of the partial reduction products. Across the whole temperature range, N_2O yields were below 12% over all of the Pd/SZ samples. At 450 °C, where maximum N_2 yield was achieved over Pd/SZ (1.0) and Pd/SZ (1.3), N_2O yields were 2.9% and 4.4%, respectively. Over all of the samples, NO yield took off at lower temperatures than N_2 yield, going through a maximum at 350 °C over Pd/SZ (0.6), Pd/SZ (1.0) and Pd/SZ (1.3). At this temperature NO yields were 44%, 55% and 64% over Pd/SZ (0.6), Pd/SZ (1.0) and Pd/SZ (1.3), respectively. Over Pd/SZ (0.3), NO yield took off at higher temperatures reaching a maximum of 67% at 400 °C. This initial increase in the NO yield is associated with partial reduction of NO_2 to NO. However, further reduction of NO to N_2 is kinetically limited in this temperature range. NO yield increased again after going through a minimum in 450–550 °C range. Above this temperature range NO yields increase since NO is the thermodynamically favored product of NO–NO_2 equilibrium. Although NO-SCR is not kinetically controlled in this temperature range, hydrocarbon combustion proceeds at a much higher rate depleting the reducing agent.

The reaction experiments carried out over Pd/SZ samples showed a parallel increase in the NO_2 reduction activity of the catalysts with the increase in the population of m-ZrO_2 sites

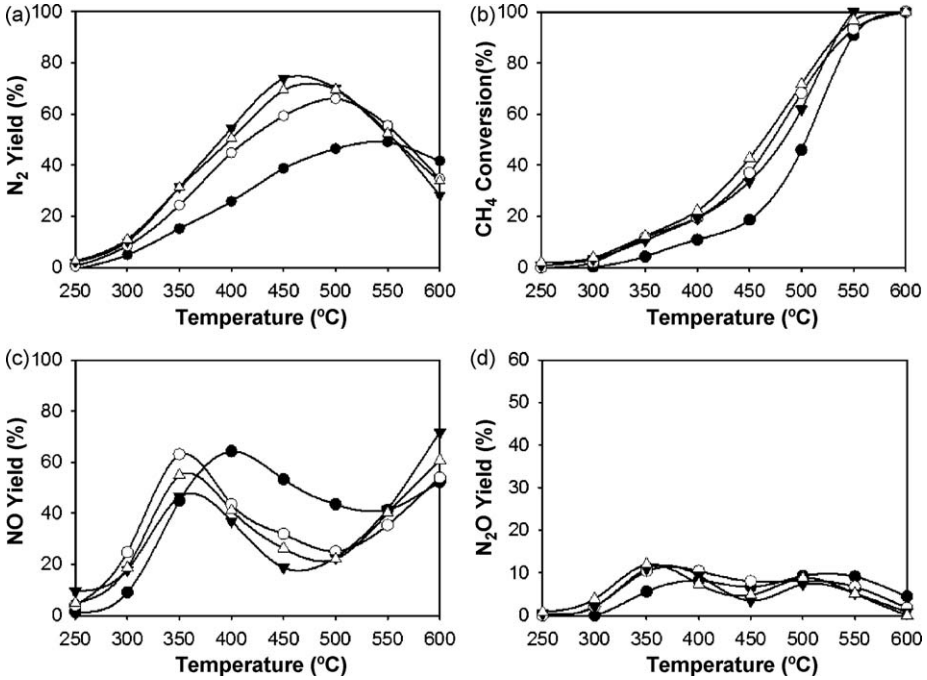

Fig. 4. NO_2 reduction with CH_4 over Pd/SZ samples. (●) Pd/SZ (0.3), (○) Pd/SZ (0.6), (▼) Pd/SZ (1.0) and (△) Pd/SZ (1.3). *Reaction conditions:* $[NO_2]$ = 1000 ppm, $[CH_4]$ = 3000 ppm and $[O_2]$ = 10% in He; 1 atm; GHSV = 20,000 h^{-1}.

although the surface population of the sulfate groups has not changed. Knozinger and co-workers [52] have reported a similar dependency of n-butane isomerization activity on the crystalline phases of ZrO_2 and showed that tetragonal phase was better suited for that reaction. For Pd-based SCR catalysts, it is well established that PdO aggregates serve as active sites for methane combustion [12,13] whereas high SCR activity has been linked to the presence of dispersed Pd^{2+} ions on the surface [17]. DRIFTS studies on Pd/H-ZSM-5 showed that pairs of Brønsted acid sites were necessary for stabilization of palladium in NO_x reduction active Pd^{2+} state. Higher NO_x reduction activity of the Pd/SZ samples prepared with higher zirconium alkoxide concentrations can be directly correlated with the presence of highly dispersed palladium phase over these catalysts, that possibly originates from different populations of ZrO_2 phases in the catalysts. Both tetragonal and monoclinic zirconia possesses octa-coordinated Zr^{4+} whereas oxygen coordination is different over the two phases. All the O^{2-} anions are tetrahedrally coordinated in t-ZrO_2 while both tetrahedrally and trigonally coordinated O^{2-} anions are present in m-ZrO_2 [53]. Through IR studies on pyridine adsorbed tetragonal and monoclinic zirconia, Zhao et al. [54] showed that both Brønsted and Lewis acid sites were found on m-ZrO_2 whereas only Lewis acid sites existed on t-ZrO_2.

NO_2 reduction experiments on Pd/SZ samples showed that SCR activity increased with increasing alkoxide concentration up to 1.0 M, above which further increase in the alkoxide concentration did not result in improvements in the activity. Pd/SZ (1.0) was further tested for activity in a dual-catalyst scheme where Co/ZrO_2 was employed as the oxidation catalyst component, to oxidize NO to NO_2 and Pd/SZ was employed as the reduction catalyst component to reduce NO_2 to N_2, as described in the next section.

3.3. Simulated lean exhaust treatment over dual-catalyst system

Fig. 5 shows a comparison of N_2 yields and CH_4 conversions as a function of temperature during simulated lean exhaust treatment with NO over Pd/SZ and a dual-catalyst bed of Pd/SZ and Co/ZrO_2 in 8:1 and 4:1 ratios. The feed stream for these experiments consisted of 400 ppm NO, 1700 ppm CH_4, 200 ppm C_2H_6, 100 ppm C_3H_8, 600 ppm CO, 6% CO_2 and 10% O_2. During simulated lean exhaust treatment over Pd/SZ insignificant N_2 yields were observed up to 350 °C above which N_2 yields took off sharply reaching yields in excess of 70% in the temperature range between 450 and 500 °C. Complete conversion of CO, C_2H_6 and C_3H_8 were achieved in the same temperature range. Methane conversion took off at slightly higher temperatures than C_2H_6 and C_3H_8. Complete conversion of methane was achieved at 550 °C. In line with our previous reports [32], complete conversion of CO was observed at temperatures as low as 250 °C (not shown). When a similar experiment was carried out with NO_2 instead of NO in the feed stream, N_2 yields took off at much lower temperatures than direct NO-SCR over the same catalyst (Fig. 5). During NO_2-SCR, the operating window shifted to lower temperatures relative to direct NO-SCR over the same catalyst and N_2 yields over 70% were achieved in 400–450 °C region. The improved activity during NO_2-SCR shows that NO_2 is easier to activate than NO for SCR over Pd/SZ.

The same experiment was carried out over mixed catalyst beds of NO_x reduction (Pd/SZ) and NO oxidation (Co/ZrO_2) catalyst component samples in 8:1 or 4:1 ratio by weight. During simulated lean exhaust treatment over a dual-catalyst bed in an 8:1 ratio, the catalyst system was able to achieve N_2 yields in excess of 90% in the 450–500 °C range. It is important to note that although N_2 yields were lower than NO_2-SCR over Pd/SZ below 450 °C the dual-catalyst system is able to outperform NO_2-SCR above 450 °C. This behavior is in line with our previous observations on incipient wetness impregnated catalysts [32]. In the presence of the oxidation catalyst component the reaction network is catalyzed in a controlled manner by generation of NO_2, which is considered to be an intermediate of NO-SCR [55,56] in close proximity to the reduction catalyst component. Due to removal of NO_2 through reduction over Pd/SZ, the NO oxidation equilibrium shifts towards products and allows achieving significantly higher N_2 yields. Furthermore, oxidation catalyst component also assumes the role of replenishing NO_2 that has been converted to NO through partial reduction.

Presence of the oxidation catalyst also resulted in significant improvements in C_xH_y conversions. During simulated lean exhaust treatment over dual-catalyst bed, CH_4 conversions were on the

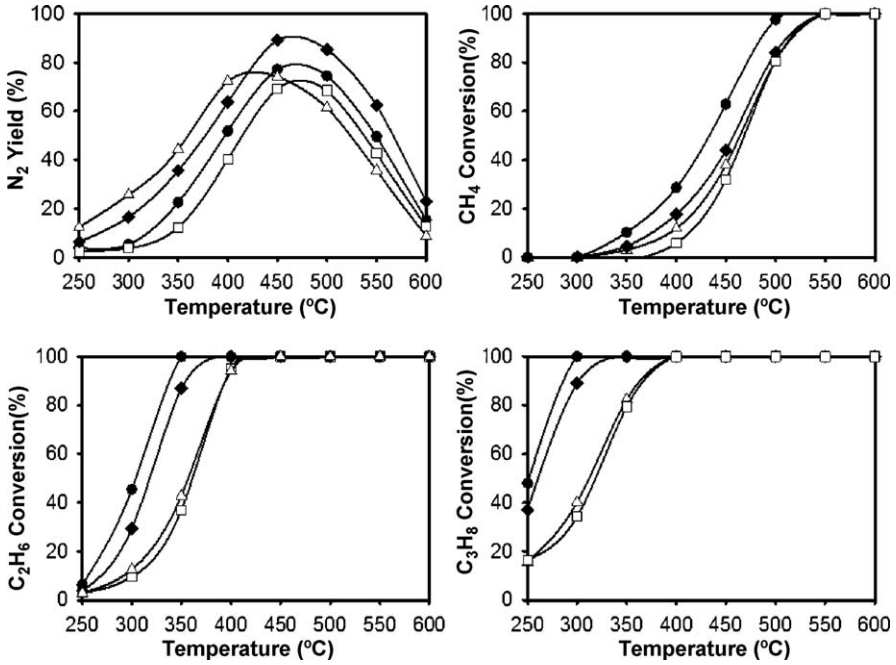

Fig. 5. Comparison of NO (□) or NO_2 reduction (△) over Pd/SZ and NO reduction over dual-catalyst beds of Pd/SZ and Co/ZrO_2 in 8:1 (◆) and 4:1 (●) ratio. *Reaction conditions:* [NO] (or [NO_2]) = 400 ppm, [CH_4] = 1700 ppm, [C_2H_6] = 200 ppm, [C_3H_8] = 100 ppm, [CO] = 600 ppm, [CO_2] = 6%, [O_2] = 10% in He; 1 atm; GHSV = 20,000 h^{-1}.

average 9% higher than simulated lean exhaust treatment over Pd/SZ in the 350–500 °C region. Similarly, in the 250–400 °C region, C_2H_6 and C_3H_8 conversions were on the average 26% and 33% higher than simulated lean exhaust treatment over Pd/SZ. In a similar experiment, the amount of oxidation catalyst component in the dual-catalyst bed was doubled while keeping the amount of reduction catalyst component constant, such that the reduction to oxidation catalyst component ratio was 4:1 by weight. Increasing the amount of oxidation catalyst in the dual-catalyst bed resulted in further improvement in hydrocarbon conversions at the expense of N_2 yield. The temperature at which complete conversion of all of the hydrocarbons was achieved shifted towards lower temperatures by approximately 50 °C. Although the N_2 yields across the whole temperature range were still on the average 6% higher than simulated lean exhaust treatment over Pd/SZ only, they were significantly lower than the dual-catalyst bed that comprised lower amount of oxidation catalyst component. A maximum N_2 yield, which was still in excess of 77%, was achieved in 450–500 °C region over this dual-catalyst bed configuration.

These results demonstrate that incorporation of small amounts of oxidation catalyst in to the Pd/SZ catalyst bed can result in significant improvements in the elimination of NO_x, carbon monoxide and unburned hydrocarbons. The results further suggest that there exists an optimum amount of oxidation catalyst that can be incorporated into the dual-catalyst system and that oxidation catalyst can also act to suppress the NO_x reduction activity of the dual-catalyst system if incorporated in excess amounts. As highlighted earlier, the hydrocarbon conversions increase with increasing oxidation catalyst amount in the dual-catalyst bed at the expense of N_2 yields. These findings are in agreement with our previous reports on the dual-catalyst scheme [32] and show that the relative contributions of oxidation and reduction catalyst components need to be optimized for each catalyst system in order to fully exploit the benefits of the dual-catalyst approach for lean exhaust treatment. The effect arises from the multifunctionality of the oxidation catalyst component. The oxidation catalyst not only oxidizes NO to NO_2 but it is also active for elimination of carbon monoxide and unburned hydrocarbons. However, increased contribution of the oxidation function in the dual-catalyst scheme tapers the efficiency of the system through the depletion of the reducing agent via the unselective route.

3.4. Effect of water vapor

Water vapor is an important constituent of lean exhaust stream and it is also generated in the aftretreatment system as a product of NO_x reduction and hydrocarbon combustion. The effect of water vapor on the lean exhaust treatment performance of Pd/SZ and dual-catalyst bed Pd/SZ and Co/ZrO_2 was investigated in the presence of different concentrations of water vapor in the exhaust stream. The effect of water vapor on the activity and stability of the oxidation catalyst component was investigated previously [35]. It was shown steady-state experiments that this catalyst was able to achieve equilibrium NO conversions at temperatures as low as 250 °C in the presence of 10% water vapor. The catalyst was further shown to exhibit stable NO oxidation activity at temperatures relevant to NO_x reduction [57].

Table 4 shows the N_2 yields achieved during NO-SCR over Pd/SZ and dual-catalyst mixed bed, NO_2-SCR over Pd/SZ and, simulated lean exhaust treatment over the dual-catalyst bed at 450 °C under steady-state conditions in the presence of water vapor at different concentrations in the feed stream. In all of the cases, an adverse effect of the presence of water vapor in the feed stream on the NO_x reduction activity was observed. Regardless of the concentration of water vapor in the feed stream, N_2 yields achieved during NO_2-SCR over Pd/SZ-only catalyst bed were higher than those achieved during direct NO-SCR over the same catalyst. These results are in agreement with our earlier findings where we have shown that water vapor would competitively adsorb with NO on Pd/SZ, whereas NO_2 adsorption would not be affected by the presence of water vapor [57].

Table 4
Comparison of N_2 yields at 450 °C during NO_2 and direct NO reduction over Pd/SZ (1.0) and dual-catalyst mixed bed in the presence of H_2O.

H_2O concentration	N_2 yield (%)			
	NO_2-SCR over Pd/SZ	Direct NO-SCR over Pd/SZ	Dual-catalyst NO-SCR	Dual-catalyst simulated lean exhaust treatment
0%	77	63	88	94
1.5%	54	41	72	81
7%	34	21	66	73

The decrease in the NO_x reduction activity in the presence of water vapor was more pronounced for reactions carried out over the reduction catalyst alone. In the presence of 7% water vapor, the N_2 yield observed during NO reduction with the dual-catalyst was three-fold higher than the N_2 yield achieved during direct NO reduction over Pd/SZ alone under the same conditions. Furthermore, in the presence of 7% water vapor, the N_2 yields achieved during NO reduction over Pd/SZ decreased from 62% to 21% while the N_2 yield decreased from 88% to 66% when the dual-catalyst bed configuration was utilized. Loss of activity with water was even less severe when simulated exhaust was used as the feed mixture over the dual-catalyst bed, still giving 73% N_2 yield. The comparison of the change in the NO_x reduction activity with the introduction of water vapor over reduction catalyst only and dual-catalyst mixed bed indicates that the presence of the oxidation catalyst component not only serves to improve the NO_x reduction activity, but also acts to offset the adverse effect of water vapor on the NO_x reduction activity. We have previously shown that presence of water vapor altered the distribution of NO_2-SCR products over Pd/SZ and favored the formation of NO and suggested that water vapor interfered with NO adsorption/retention on the Pd/SZ surface through a competitive adsorption phenomena whereas, NO_2 adsorption was not affected by the presence of water vapor [57]. The oxidation catalyst component would offset the effect of water vapor by re-oxidizing the partially reduced NO back to NO_2 and thus, result in improved N_2 yields.

4. Conclusions

Sol–gel prepared Pd/SZ catalysts were investigated for application in a novel multi-functional catalytic strategy for simultaneous elimination of NO_x, carbon monoxide and unburned hydrocarbons in lean-burn natural gas reciprocating engine exhaust. Over this catalytic system NO_x reduction is achieved in two mechanistic steps, where NO is first oxidized to NO_2 over an oxidation catalyst component and NO_2 is reduced to N_2 over a reduction catalyst component. Zirconium alkoxide concentration in the sol was varied during catalyst preparation in order to exert control on catalyst morphology. Presence of both tetragonal and monoclinic ZrO_2 crystal phases was identified through XRD. Both the fraction and crystallite size of m-ZrO_2 phase increased with increasing alkoxide concentration. Additionally, increasing alkoxide concentration led to an increase in the palladium dispersion over the catalyst samples possibly through stabilization of palladium in the form Pd^{2+} ions by Brønsted acid sites of m-ZrO_2. In line with the increase in Pd dispersion the NO_2-SCR activity of the Pd/SZ samples increased with increasing alkoxide concentration. The best performing Pd/SZ samples was tested as the reducing catalyst

component in the integrated dual-catalyst scheme. Addition of water vapor to the feed stream caused significant decrease in the activity of Pd/SZ however, when NO_x reduction is carried out over the dual-catalyst mixed bed, the presence of the oxidation catalyst component acted to offset the effect of water vapor.

Acknowledgements

Financial support provided by US Department of Energy is gratefully acknowledged. The authors also acknowledge NSF support for acquisition of the XPS system under NSF-DMR grant #0114098.

References

[1] G.R. Gerber, M.A. Devine, Efficiency emissions advances keep recip engines in the DG mix, Power 147 (2003) 24–29.
[2] R.M. Heck, Catalytic abatement of nitrogen oxides-stationary applications, Catal. Today 53 (1999) 519–523.
[3] M. Iwamoto, H. Hamada, Removal of nitrogen monoxide from exhaust gases through novel catalytic processes, Catal. Today 10 (1991) 57–71.
[4] M. Iwamoto, H. Yahiro, Novel catalytic decomposition and reduction of NO, Catal. Today 22 (1994) 5–18.
[5] Y. Nishizaka, M. Misono, Catalytic reduction of nitrogen monoxide by methane over palladium-loaded zeolites in the presence of oxygen, Chem. Lett. 22 (1993) 1295–1298.
[6] Y. Nishizaka, M. Misono, Essential role of acidity in the catalytic reduction of nitrogen monoxide by methane in the presence of oxygen over palladium-loaded zeolites, Chem. Lett. 23 (1994) 2237–2240.
[7] C.M. De Correa, F. Cordoba C., F. Bustamante L., Cooperation of Pt and Pd over H-mordenite for the lean SCR of NO_x by methane, Stud. Surf. Sci. Catal. 130B (2000) 1469–1474.
[8] C. Descorme, P. Gelin, C. Lecuyer, M. Primet, Catalytic reduction of nitric oxide by methane in the presence of oxygen on palladium-exchanged mordenite zeolites, J. Catal. 177 (1998) 352–362.
[9] L.J. Lobree, A.W. Aylor, J.A. Reimer, A.T. Bell, NO Reduction by CH_4 in the Presence of O_2 over Pd-H-ZSM-5, J. Catal. 181 (1999) 189–204.
[10] M. Ogura, M. Hayashi, S. Kage, M. Matsukata, E. Kikuchi, Determination of active palladium species in ZSM-5 zeolite for selective reduction of nitric oxide with methane, Appl. Catal. B: Environ. 23 (1999) 247–257.
[11] M. Ogura, M. Hayashi, E. Kikuchi, Role of zeolite structure on reduction of NO_x with methane over In- and Pd-based catalysts, Catal. Today 45 (1998) 139–145.
[12] R. Burch, Low NO_x options in catalytic combustion and emission control, Catal. Today 35 (1997) 27–36.
[13] H. Ohtsuka, T. Tabata, Effect of water vapor on the deactivation of Pd-zeolite catalysts for selective catalytic reduction of nitrogen monoxide by methane, Appl. Catal. B: Environ. 21 (1999) 133–139.
[14] J.A.Z. Pieterse, R.W. Brink, S. Booneveld, F.A. de Bruijn, Durability of ZSM5-supported Co-Pd catalysts in the reduction of NO_x with methane, Appl. Catal. B: Environ. 39 (2002) 167–179.
[15] J. Suzuki, S. Matsumoto, Development of catalysts for diesel particulate NO_x reduction, Top. Catal. 28 (2004) 171–176.
[16] H. Ohtsuka, T. Tabata, T. Hirano, Palladium–platinum-loaded sulfated zirconia: a highly durable catalyst for the reduction of nitrogen oxides by methane in the presence of water vapor and SO_x, Appl. Catal. B: Environ. 28 (2000) L73–L76.
[17] A. Ali, W. Alvarez, C.J. Loughran, D.E. Resasco, State of Pd on H-ZSM-5 and other acidic supports during the selective reduction of NO by CH_4 studied by EXAFS/XANES, Appl. Catal. B 14 (1997) 13–22.
[18] Y.-H. Chin, A. Pisanu, L. Serventi, W. Alvarez, D.E. Resasco, NO reduction by CH_4 in the presence of excess O_2 over Pd/sulfated zirconia catalysts, Catal. Today 54 (1999) 419–429.
[19] S. Ardizzone, C.L. Bianchi, E. Grassi, The role of oxide precursor on the features of sulphated zirconia, Colloid Surf. A 135 (1998) 41–51.
[20] D.R. Milburn, R.A. Keogh, R. Srinivasan, B.H. Davis, Pt-SO_4^{2-}-ZrO_2 catalysts. Correlation of catalytic activity with SO_4^{2-} XPS data, Appl. Catal. A: Gen. 147 (1996) 109–125.
[21] S. Ardizzone, C.L. Bianchi, Acidity, sulphur coverage and XPS analyzes of ZrO_2-SO_4 powders by different procedures, Appl. Surf. Sci. 152 (1999) 63–69.
[22] K. Ebitani, H. Konno, T. Tanaka, H. Hattori, In-situ XPS study of zirconium oxide promoted by platinum and sulfate ion, J. Catal. 135 (1992) 60–67.
[23] D.A. Ward, E.I. Ko, One-step synthesis and characterization of zirconia-sulfate aerogels as solid superacids, J. Catal. 150 (1994) 18–33.
[24] D. Tichit, B. Coq, H. Armendariz, F. Figueras, One-step sol–gel synthesis of sulfated-zirconia catalysts, Catal. Lett. 38 (1996) 109–113.
[25] D.A. Ward, E.I. Ko, Sol–gel synthesis of zirconia supports: important properties for generating n-butane isomerization activity upon sulfate promotion, J. Catal. 157 (1995) 321–333.
[26] L.B. Hamouda, A. Ghorbel, Control preparation of sulfated zirconia by sol–gel process: impact on catalytic performances during n-hexane isomerization, J. Sol–Gel Sci. Technol. 19 (2000) 413–416.
[27] H. Armendariz, B. Coq, D. Tichit, R. Dutartre, F. Figueras, Influences of some synthesis parameters and activation procedures on the one-step sol–gel synthesis of sulfated-zirconia catalysts, followed by TG–DSC and mass spectrometry, J. Catal. 173 (1998) 345–354.
[28] M. Signoretto, L. Oliva, F. Pinna, G. Strukul, Synthesis of sulfated-zirconia aerogel: effect of the chemical modification of precursor on catalyst porosity, J. Non-Cryst. Solids 290 (2001) 145–152.
[29] L.B. Hamouda, A. Ghorbel, New process to control hydrolysis step during sol–gel preparation of sulfated zirconia catalysts, J. Sol–Gel Sci. Technol. 39 (2006) 123–130.
[30] E.M. Holmgreen, M.M. Yung, U.S. Ozkan, Pd-based sulfated zirconia prepared by a single step sol–gel procedure for lean NO_x reduction, J. Mol. Catal. A: Chem. 270 (2007) 101–111.
[31] M. Signoretto, F. Pinna, G. Strukul, G. Cerrato, C. Morterra, Platinum promoted zirconia-sulfate catalysts: one-pot preparation, physical properties and catalytic activity, Catal. Lett. 36 (1996) 129–133.
[32] E.M. Holmgreen, M.M. Yung, U.S. Ozkan, Dual-catalyst aftertreatment of lean-burn natural gas engine exhaust, Appl. Catal. B: Environ. 74 (2007) 73–82.
[33] U.S. Ozkan, E.M. Holmgreen, M.M. Yung, Multi-stage catalyst systems and uses thereof, US20070110651.
[34] J. Despres, M. Elsener, M. Koebel, O. Krocher, B. Schnyder, A. Wokaun, Catalytic oxidation of nitrogen monoxide over Pt/SiO_2, Appl. Catal. B 50 (2004) 73–82.
[35] M.M. Yung, E.M. Holmgreen, U.S. Ozkan, Cobalt-based catalysts supported on titania and zirconia for the oxidation of nitric oxide to nitrogen dioxide, J. Catal. 247 (2007) 356–367.
[36] E.M. Holmgreen, M.M. Yung, U.S. Ozkan, Pd-supported on sulfated monoclinic zirconia for the reduction of NO_2 with methane under lean conditions, Catal. Lett. 111 (2006) 19–26.
[37] H. Toraya, M. Yoshimura, S. Somiya, Calibration curve for quantitative analysis of the monoclinic-tetragonal ZrO_2 system by X-ray diffraction, J. Am. Ceram. Soc. 67 (1984) C119–C121.
[38] L. Maffucci, P. Iengo, M. Di Serio, E. Santacesaria, A rapid method for the evaluation of the dispersion of palladium in supported catalysts, J. Catal. 172 (1997) 485–487.
[39] J.E. Bailey, D. Lewis, Z.M. Librant, L.J. Parker, Phase transformations in milled zirconia, Trans. Br. Ceram. Soc. 71 (1972) 25–30.
[40] P.D.L. Mercera, J.G. van Ommen, E.B.M. Doesburg, A.J. Burggraaf, J.R.H. Ross, Stabilized tetragonal zirconium oxide as a support for catalysts: evolution of the texture and structure on calcination in static air, Appl. Catal. 78 (1991) 79–96.
[41] R. Guinebretiere, A. Dauger, A. Lecomte, H. Vesteghem, Tetragonal zirconia powders from the zirconium n-propoxide-acetylacetone–water–isopropanol system, J. Non-Cryst. Solids 147–148 (1992) 542–547.
[42] T. Itoh, Crystallite growth of ZrO_2 powder, J. Mater. Sci. Lett. 4 (1985) 1029–1032.
[43] R.C. Garvie, The occurrence of metastable tetragonal zirconia as a crystallite size effect, J. Phys. Chem. 69 (1965) 1238–1243.
[44] Y.-H. Chin, W. Alvarez, D.E. Resasco, Sulfated zirconia and tungstated zirconia as effective supports for Pd-based SCR catalysts, Catal. Today 62 (2000) 159–165.
[45] P. Bautista, M. Faraldos, M. Yates, A. Bahamonde, Influence of sulphate doping on Pd/zirconia based catalysts for the selective catalytic reduction of nitrogen oxides with methane, Appl. Catal. B 71 (2007) 254–261.
[46] D. Farcasiu, J. Qi Li, S. Cameron, Preparation of sulfated zirconia catalysts with improved control of sulfur content. II. Effect of sulfur content on physical properties and catalytic activity, Appl. Catal. A 154 (1997) 173–184.
[47] L.-F. Yang, Y.-X. Hu, D. Jin, X.-E. He, C.-K. Shi, J.-X. Cai, Effect of support structure on methane combustion over PdO/ZrO_2, Stud. Surf. Sci. Catal. 147 (2004) 469–474.
[48] J.F. Moulder, W.F. Stickle, P.E. Sobol, K.D. Bomben, Handbook of X-Ray Photoelectron Spectroscopy, PerkinElmer Corporation, Eden Prairie, 1992.
[49] K. Arata, Solid superacids, Adv. Catal. 37 (1990) 165–212.
[50] C.L. Bianchi, S. Ardizzone, G. Cappalletti, Surface state of sulfated zirconia: the role of the sol–gel reaction parameters, Surf. Interface Anal. 36 (2004) 745–748.
[51] M. Hino, M. Kurashige, H. Matsuhashi, K. Arata, The surface structure of sulfated zirconia: studies of XPS and thermal analysis, Themochim. Acta 411 (2006) 35–41.
[52] W. Stichert, F. Schluth, S. Kuba, H. Knozinger, Monoclinic and tetragonal high surface area sulfated zirconias in burane isomerization: CO adsorption and catalytic results, J. Catal. 198 (2001) 277–285.
[53] K.-H. Jacob, E. Knozinger, S. Benier, Adsorption sites on polymorphic zirconia, J. Mater. Chem. 3 (1993) 651–657.
[54] Y. Zhao, W. Li, M. Zhang, K. Tao, A comparison of surface acidic features between tetragonal and monoclinic nanostructured zirconia, Catal. Commun. 3 (2002) 239–245.
[55] T. Tabata, M. Kokitsu, H. Ohtsuka, O. Okada, L.M.F. Sabatino, G. Bellussi, Study on catalysts of selective reduction of NO_x using hydrocarbons for natural gas engines, Catal. Today 27 (1996) 91–98.
[56] B.J. Adelman, T. Beutel, G.D. Lei, W.M.H. Sachtler, Mechanistic cause of hydrocarbon specificity over Cu/ZSM-5 and Co/ZSM-5 catalysts in the selective catalytic reduction of NO_x, J. Catal. 158 (1996) 327–335.
[57] B. Mirkelamoglu, U.S. Ozkan, Dual catalyst aftertreatment of lean-burn natural gas engine exhaust: hydrothermal stability of Pd/SZ, Appl. Catal. B: Environ., accepted for publication.